Soft Matter

Accepted Manuscript

ROYAL SOCIETY OF CHEMISTRY

www.rsc.org/softmatter

Journal Name

RSCPublishing

ARTICLE

Discovery of a Tetracontinuous, Aqueous Lyotropic Network Phase with Unusual 3D–Hexagonal Symmetry

Cite this: DOI: 10.1039/x0xx00000x

Received ooth January 2014,
Accepted ooth January 2014

DOI: 10.1039/x0xx00000x

www.rsc.org/

Gregory P. Sorenson, Adam K. Schmitt, and Mahesh K. Mahanthappa*

Network phase aqueous lyotropic liquid crystals (LLCs) are technologically useful materials with myriad applications in chemistry, biology, and materials science, which stem from their structurally periodic aqueous and hydrophobic nanodomains (~0.7–5.0 nm in diameter) that are lined with well–defined chemical functionalities. To date, the exclusive observation of bicontinuous cubic network phase LLCs (*e.g.*, double gyroid, double diamond, and primitive phases) has fueled speculations that all stable LLC network phases must exhibit cubic symmetry. Herein, we describe the self–assembly behavior of a simple aliphatic gemini surfactant that forms the first example of a triply periodic network phase LLC with the 3D–hexagonal symmetry $P6_3/mcm$ (space group #193). This normal, tetracontinuous 3D–hexagonal network LLC phase H_1^{193} partitions space into four continuous and interpenetrating, yet non–intersecting volumes. This discovery directly demonstrates that the gemini amphiphile platform furnishes a rational strategy for discovering and stabilizing new, three–dimensionally periodic multiply continuous network phase LLCs with variable symmetries and potentially new applications.

Introduction

The concentration–dependent self–assembly of small molecule amphiphiles into lyotropic liquid crystals (LLCs), comprising structurally periodic aqueous and hydrophobic nanodomains (~0.7–5 nm in diameter) lined with well–defined chemical functionalities, has wide-ranging implications in chemistry, materials science, and biology.[1] Common LLC morphologies include cubic micellar (I), hexagonally packed cylinders (C), and lamellar (L_α) phases. In typically narrow temperature and amphiphile concentration windows situated between the C and L_α phases, hydrated surfactants form complex ordered network phase LLCs.[2-4] These three–dimensionally periodic structures are comprised of two or more continuous and interpenetrating networks of hydrophobic and aqueous nanodomains. Three highly symmetric, tricontinuous network phase LLCs with cubic symmetry (Q–phases) are ubiquitous (Fig. 1): double gyroid (G; $Ia\bar{3}d$ symmetry), double diamond (D; $Pn\bar{3}m$ symmetry), and primitive (P; $Im\bar{3}m$ symmetry).[5] These triply periodic Q–phase LLCs are a focal point for the development of membranes for molecular separations and selective ion transport in fuel cells and batteries,[6, 7] and as templates for mesoporous inorganic materials.[8, 9] Bicontinuous "lipidic cubic phase" LLCs have also enabled the crystallization and X–ray

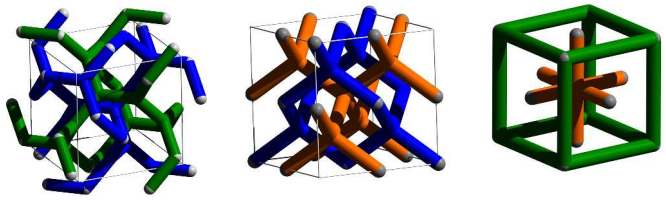

Fig 1. Wireframe depictions of the network connectivities of commonly observed Q–phase LLC morphologies with cubic symmetries (*left to right*): the double gyroid (G; $Ia\bar{3}d$ symmetry), double diamond (D; $Pn\bar{3}m$ symmetry), and primitive (P; $Im\bar{3}m$ symmetry), which are comprised of two interpenetrating networks of either three–, four–, or six–fold connectors, respectively.

structure determination of important integral transmembrane proteins, including G–protein coupled receptors (GPCRs).[10, 11] Recent work has further established the utility of Q–phase LLCs in the delivery of both therapeutic siRNAs[12] and small molecules.[13]

Given that many surfactants form aqueous Q–phase LLCs, conventional wisdom suggests that cubic symmetries must underlie *all* stable triply periodic multiply continuous aqueous LLCs.[14] This notion stems from the fact that G, D, and P LLCs maybe derived from arranging surfactant molecules along the high symmetry Schöen G, Schwarz D, and Schwarz P triply periodic minimal surfaces (TPMS), respectively, to yield LLC morphologies exhibiting negative Gaussian ("saddle splay") curvature.[15] These molecular arrangements minimize packing frustration in the resulting assemblies that exhibit mean interfacial curvatures in between those of the C and L_α phases. In spite of theoretical predictions of the existence of stable, non–cubic LLC network phases derived from non–cubic TPMS,[14, 16] no such network phases in simple lipid/water mixtures have been observed.

Herein, we describe the first example of a triply periodic network phase aqueous LLC with the 3D-hexagonal $P6_3/mcm$ symmetry (space group #193) derived from a simple, aliphatic dicarboxylate gemini surfactant. This tetracontinuous hexagonal network phase H_I^{193} partitions space into four continuous and interpenetrating, yet non–intersecting volumes. This unusual thermodynamic equilibrium nanostructure exhibits an interfacial curvature intermediate between that of the C and G phases, consistent with previous theoretical predictions by Schröeder–Turk et al.[14] The discovery that this simple gemini ("twin tail") surfactant architecture enables access to the H_I^{193} phase suggests a powerful molecular design strategy for synthesizing amphiphiles that stabilize new families of non–cubic LLCs with potentially useful properties.

Experimental

Materials

All materials and reagent grade solvents were purchased from the Sigma–Aldrich Chemical Co. (Milwaukee, WI) and used as received unless otherwise noted. 1,4–dibromobutane and 1,6–dibromohexane were distilled and stored under nitrogen. Diisopropylamine (Sigma–Aldrich) was distilled from CaH_2 and stored under nitrogen. Hexamethylphosphoramide (HMPA) was distilled from CaH_2 and stored over 4 Å molecular sieves. *n*–Butyllithium in hexanes was titrated using diphenylacetic acid in THF. Anhydrous and anaerobic THF was obtained by nitrogen degassing of analytical grade solvent for 30 min, followed by cycling through a column of activated alumina in a Vacuum Atmospheres Solvent purification system. The synthesis of disodium docosane–9,14–dicarboxylate (**Na–74**) was previously reported.[17]

Molecular characterization

^{1}H NMR and ^{13}C NMR spectra were recorded in DMSO–d_6 or methanol–d_4 at 25 °C on both Varian MercuryPlus 300 and Bruker AC+ 300 spectrometers; spectra were referenced to the residual protiated solvent peaks in the samples. Mass spectrometry was performed using a Waters (Micromass) LCT® electrospray ionization time–of–flight mass spectrometer operating in negative ion detection mode. Samples dissolved in CH_3OH were sprayed with a sample cone voltage of 20 V. IR spectra were recorded on a Bruker Tensor FTIR from 4000–500 cm^{-1}, using a diamond crystal attenuated total reflectance (ATR) stage. Elemental analysis (C, H, N) were performed by Columbia Analytical Services (Tuscon, AZ), using Combustion/TC and IR detection.

Hexacosane–11,16–dicarboxylic acid

A 500 mL 2–necked round bottom flask fitted with an addition funnel was charged with a stirbar, THF (200 mL), and diisopropylamine (14.7 mL, 105 mmol) under $N_2(g)$. Upon cooling this solution to –15 °C in an ethanol/H_2O/dry ice bath, *n*–BuLi (36.8 mL of 2.78 M solution in hexanes, 102 mmol) was added dropwise via addition funnel. The reaction mixture was stirred for 30 min, after which a solution of dodecanoic acid (10.01 g, 49.97 mmol) in THF (50.0 mL) was added dropwise via addition funnel. HMPA (8.68 mL, 49.9 mmol) was then added, and the stirred reaction mixture was warmed to 22 °C for 30 min. The reaction mixture was again cooled to –15 °C, and 1,4–dibromobutane (2.90 mL, 24.4 mmol) was added dropwise. The reaction was then allowed to warm to 22 °C and stirred for 14 h. The reaction was quenched by the addition of cold 10% HCl (*aq*) (100 mL), transferred to a separatory funnel, and the aqueous and organic layers were separated. The aqueous layer was extracted with ether (3 x 50 mL) and the combined organic layers were washed with 10% HCl (3 x 50 mL), water (50 mL), and saturated NaCl (*aq*) (50 mL). After drying over $MgSO_4(s)$, all volatiles were removed under vacuum. The crude solid was purified by recrystallization from EtOH. Yield: 9.29 g (84%); ^{1}H NMR (300 MHz, DMSO–d_6): δ 11.96 (2H, s, COO*H*), 2.15 (2H, m, C*H*–COOH), 1.56–1.08 (44H, m, CH_2), 0.848 (6H, t, $J_{H\text{-}H}^3$ = 7.0 Hz, CH_2–CH_3). ^{13}C NMR (75.4 MHz, DMSO–d_6): δ 177.3 (C=O), 45.14 (CH), 32.21 (CH_2), 32.17 (CH_2), 32.04 (CH_2), 31.72 (CH_2), 29.39 (CH_2x2), 29.31 (CH_2), 29.13 (CH_2), 27.24 (CH_2), 27.18 (CH_2), 22.50 (CH_2), 14.28 (CH_3). MS (ESI–TOF) calcd. *m/z* for $C_{24}H_{45}O_4^-$ 453.4, found: 453.4.

Disodium hexacosane–11,16–dicarboxylate (Na–94)

In a flask equipped with a stirbar, hexacosane–11,16–dicarboxylic acid (2.505 g, 5.508 mmol) and Na_2CO_3 (0.584 g, 5.51 mmol) were suspended in CH_3OH (55.0 mL). The mixture was stirred at 22 °C until it became homogeneous, and then stirring was continued for 1 h. All volatiles were removed under vacuum, and residual water and methanol were azeotropically distilled using C_6H_6 three times under vacuum. Yield: 2.75 g (quant.). ^{1}H NMR (300 MHz, CD_3OD): δ 2.14

(2H, m, C*H*–COO$^-$), 1.53 (4H, m, CH–CH_2), 1.43–1.13 (40 H, m, CH_2), 0.894 (6H, t, $J_{H\text{-}H}{}^3$ = 7.0 Hz, 6H CH_2–CH_3). ^{13}C NMR (75.4 MHz, CD_3OD): δ 184.1 (C=O), 49.49 (CH), 33.40 (CH_2), 33.25 (CH_2 x 2), 31.59 (CH_2), 29.59 (CH_2), 29.32 (CH_2 x 2), 28.99 (CH_2), 28.08 (CH_2), 27.71 (CH_2), 22.25 (CH_2), 12.95 (CH_3). *Anal.* Calc.: $C_{28}H_{52}O_4Na_2$: C, 67.44; H, 10.51; Found: C, 67.02; H, 10.15.

Lyotropic Phase Sample Preparation

Aqueous lyotropic liquid crystal (LLC) samples were prepared for X–ray scattering analysis by weighing appropriate amounts of rigorously dried Gemini salt and doubly distilled water into a vial and centrifuging the tightly capped mixture for 10 min, manual mixing using a spatula, and an additional 10 min of centrifugation. After centrifugation, the samples were allowed to rest at 22 °C for at least 12 h prior to X–ray analysis. Samples were stored in tightly sealed vials whenever possible during sample preparation, in order to minimize water loss through evaporation.

Small–angle X–Ray Scattering

Synchrotron small–angle X–ray scattering (SAXS) measurements were performed at the 12–ID–B beamline at the Advanced Photon Source (Argonne, IL). Experiments employed a beam energy of 12 keV (λ = 1.034 Å) and a 2.550 m sample–to–detector distance, which was calibrated using a silver behenate standard sample with d = 58.38 Å. Two–dimensional SAXS patterns were recorded on a Pilatus 2M detector (25.4 cm x 28.9 cm rectangular area) with 1475 x 1679 pixel resolution. Mounted in aluminium DSC pans, LLC samples were heated to a desired temperature in a Linkam DSC hot stage and allowed to equilibrate for 5 min prior to data collection (exposure time ~1 s). 2D patterns were azimuthally integrated to obtain Log(Intensity(q)) *v.* q plots using the DataSqueeze software package (http://www.datasqueezesoftware.com/).

Detailed analysis and pattern indexing of synchrotron SAXS data employed the Jade 5 software package (Materials Data, Inc., Livermore, CA). Rietveld refinement was conducted using the *JANA2006*[18] software package to extract structure factor intensities and peak full–width at half maxima associated with each allowed SAXS peak for LLC phases of interest. From these data, we generated a text file input for use with the charge–flipping alogorithm *SUPERFLIP*[19] to obtain an electron density reconstruction based on the SAXS data.

Rheological Measurements

Frequency-dependent storage (G') and loss (G") moduli of LLCs were measured using a TA Instruments ARES–LS2 rheometer in strain–controlled mode at 25 and 55 °C. All measurements were performed in a parallel–plate geometry with a 50 mm Peltier temperature–controlled bottom plate and a 8 mm top plate. To minimize water loss from the samples, a collar with a water–saturated sponge was fitted onto the bottom plate to surround the sample without making contact with the upper plate fixture or the sample. Dynamic strain sweep measurements were performed over the range |γ| = 0.03–1% with ω = 0.1 Hz at 12 logarithmically spaced values in order to identify the linear viscoelastic regime of the material. Dynamic frequency sweep measurements were then performed at |γ| = 0.1% at 19 logarithmically spaced frequencies with 0.01≤ ω ≤ 50 Hz.

Results & Discussion

Gemini amphiphiles, derived from linking two single–tail surfactants at or near their hydrophilic headgroups, exhibit an increased propensity to form G–phase LLCs in water.[20-22] Recently, we reported that anionic gemini dicarboxylate amphiphiles (Scheme 1) form unusually stable, normal double gyroid (G_I) LLC phases over large amphiphile concentration windows up to 20 wt% wide with unexpected thermal stabilities over the range T = 25–100 °C.[17] Our studies of decanoic acid–derived surfactants such as **Na–74** highlighted the sensitive dependence of the cubic G_I–phase stability on the identity of the hydrophilic headgroup, the nature of the headgroup–counterion interaction, and the structure of the aliphatic surfactant scaffold. Subsequent molecular dynamics simulations of these self–assembled phases have demonstrated that these aliphatic gemini dicarboxylates adopt splayed chain molecular conformations, the subtle supramolecular packings of which are electrostatically controlled by the extent of counterion–headgroup dissociation at a given hydration level.[23]

In the course of our extended studies of the LLC phase

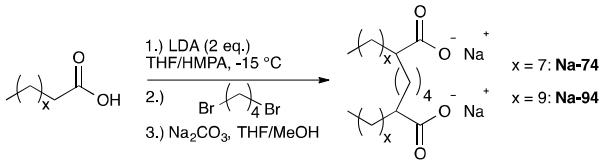

Scheme 1. Synthesis of Aliphatic Gemini Dicarboxylate Surfactants.

behavior of gemini dicarboxylate surfactants, we were led to investigate the effects of hydrophobic tail length on the unusual supramolecular self–assembly of these molecules. Consequently, we synthesized the gemini surfactant **Na–94** derived from dodecanoic acid and 1,4–dibromobutane in high yields according to Scheme 1. Using temperature–dependent small–angle X–ray scattering (SAXS), we investigated the LLC phases formed by variably hydrated samples of **Na–94** over the concentration range 30–100 wt% amphiphile in H_2O between T = 22–100 °C. We assigned the resulting LLC morphologies based on the positions of the observed SAXS peaks according to well–documented methods.[4,17] For example, the azimuthally–integrated SAXS patterns shown in Fig. 2a and 2d at 50 and 65 wt% **Na–94** correspond to H and G phase LLCs, respectively. The results of our SAXS analyses are summarized in the temperature versus amphiphile concentration LLC phase diagram shown in Fig. 3. Below 40 wt% **Na–94** in H_2O, micellar solutions with no periodic long–range order form. Upon systematically decreasing the water content, we noted

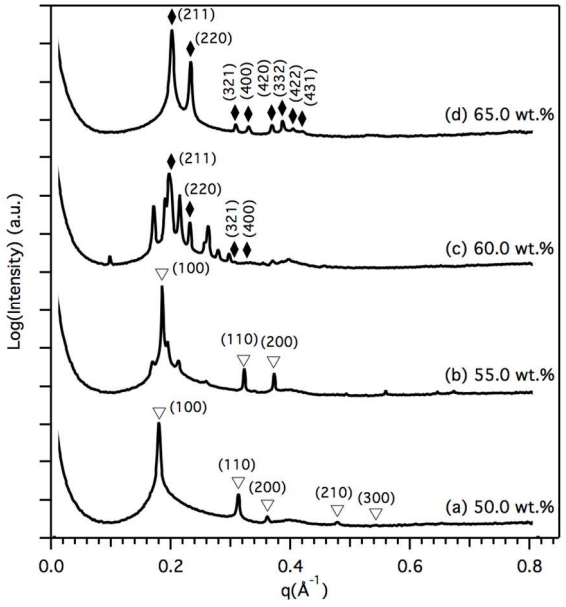

Fig. 2. Azimuthally–integrated synchrotron SAXS patterns for aqueous LLCs derived from **Na–94** in the composition range 50.0–65.0 wt% **Na–94** in H_2O at 30 °C, where diamonds (♦) and open triangles (▽) denote the expected peak positions for the gyroid (G_I) and cylinders (C_I) morphologies, respectively, along with their associated Miller indices.

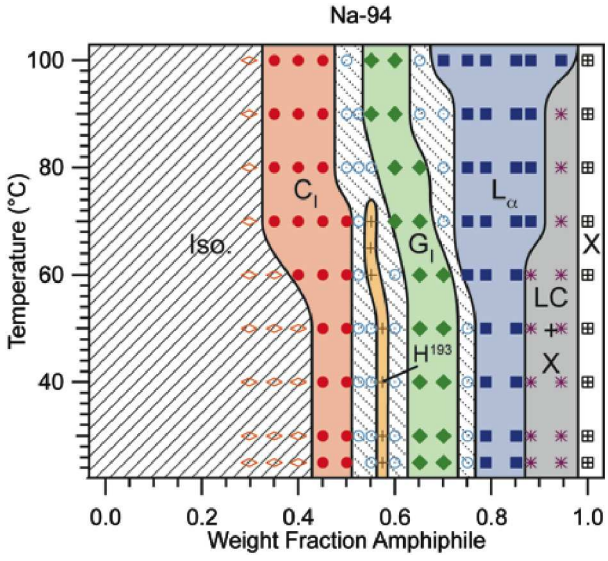

Fig. 3. Lyotropic liquid crystal phase diagram for **Na–94** in H_2O illustrating the formation of lamellae (L_α), hexagonally–packed cylinders (C_I), gyroid (G_I) phases, as well as the new H_I^{193} phase at intermediate compositions. The isotropic (Iso) phase window refers to micellar solutions that lack periodic long–range order, and the open circles (⊙) refer to windows of LLC phase coexistence of the adjacent pure phases.

that **Na–94** forms an unusual sequence of composition–dependent LLC phases: C → unknown → G → L_α. Since the C, G, and unknown phases occur at higher water contents than the zero–curvature L_α phase formed by **Na–94**, we deduce that interfacial curvature toward the lipid domains is favored. Thus, these are "normal" (Type I) LLC phases in which water is the majority phase.

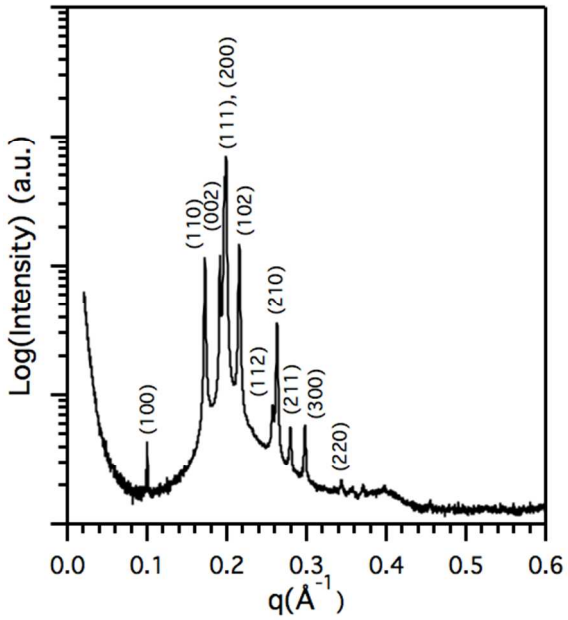

Fig. 4. Representative synchrotron SAXS pattern for the LLC derived from **Na-94** at a composition of 57.5 wt% **Na-94** at 40 °C, which exhibits a pure H_I^{193} phase. The first 11 peaks are labelled with the Miller indices expected for the *P6₃/mcm* symmetry with unit cell parameters a = 7.37 nm and c = 6.63 nm (c/a = 0.900); detailed pattern indexing is given in Figure S2 and Table S1.

In the composition range 52–60 wt% **Na–94** in $H_□O$, we recorded a series of SAXS patterns that exhibit peak positions and a scattering intensity envelope inconsistent with any known phase coexistence or any previously reported LLC structure. The composition–dependent progression of SAXS patterns shown in Fig. 2 illustrates the formation of a new, unidentified phase in nearly pure form near 60 wt% **Na–94** in water at 25 °C. A sample of 57.5 wt% **Na–94** in water at 40 °C forms a pure phase that exhibits the SAXS pattern shown in Fig. 4, in which the relative positions of the observed peaks occur at approximately $q/q^* \approx \sqrt{(4/3)}, \sqrt{4}, \sqrt{5}, \sqrt{(47/9)}, \sqrt{(16/3)}, \sqrt{(25/4)}, \sqrt{9}, \sqrt{(28/3)}, \sqrt{(95/9)}, \sqrt{12}, \sqrt{16}$ with $q^* = 0.0856$ Å^{-1} (see Table S1 for detailed listing of the observed peak positions). Qualitatively, the apparently homogenous optical birefringence of this new phase implies its underlying non–cubic symmetry. Near 80 °C, SAXS analyses also indicate that this new LLC phase undergoes a thermoreversible order–order phase transition to the cubic G_I–phase (Fig. S1), which suggests the thermodynamic equilibrium nature of this new LLC phase.

The observed SAXS peak positions for this new phase are consistent with the three–dimensional hexagonal space group symmetry $P6_3/mcm$ (space group #193), denoted H_I^{193} wherein the subscript designates a Type I phase, with unit cell dimensions c = 6.63 nm and a = 7.37 nm (c/a = 0.900). Table S1 contains a complete list of 20 observed scattering peak positions, their corresponding Miller indices, and the calculated residuals that are in exceptional agreement with the expected values (≤ 0.004° deviation). While the $P3c1$, $P\bar{3}c1$, $P6_3cm$, and $P\bar{6}c2$ symmetries also produce the same scattering signature,

we favor the highest symmetry $P6_3/mcm$ space group per crystallographic convention.[24] The Miller indices associated with the peaks in the azimuthally–integrated one–dimensional scattering intensity profile are given in Fig. 4 (see also Fig. S2).

SAXS patterns associated with LLC samples comprising 55.0 and 60 wt% **Na–94** in water over the temperature range 30–65 °C are consistent with H_I^{193} phase coexistence with either of the adjacent C_I or G_I phases (Fig. 2). The notable lack of C_I/G_I phase coexistence below 70 °C at any concentration implies that the H_I^{193} structure is a new, equilibrium LLC mesophase. In a LLC composition window similarly situated between the C_I and G_I phases, we note that the structurally homologous gemini surfactant **Na–74** exhibits a similar previously unassigned phase coexistence of G_I and H_I^{193} phases near 55 wt% surfactant in H_2O (Fig. S3).[17] For the **Na–74** samples, we also deduce a similar unit cell ratio $c/a = 0.91$.

The percolating aqueous and hydrophobic domain structures associated with triply periodic network phase LLCs manifest in their solid–like linear viscoelastic rheological properties. Mezzenga *et al.* demonstrated that inverse (Type II) bicontinuous cubic G_{II} and D_{II} LLCs typically exhibit large and nearly frequency–independent dynamic elastic storage shear moduli $G'(\omega) \approx 0.5–1$ MPa over broad frequency ranges.[25] Consistent with this notion, the G_I–phase formed by 60 wt% **Na–94** in H_2O exhibits a frequency–independent $G'(\omega) \approx 10$ MPa at 25 °C (Fig. S4). However, the discontinuous C_I–phase formed at 50 wt% **Na–94** exhibits a much lower $G'(\omega) \approx 0.1$ MPa at 25 °C, which is notably frequency dependent (Fig. S5). Dynamic elasticity measurements reveal that the H_I^{193} phase exhibits a substantial $G'(\omega) \approx 1$ MPa, which is relatively insensitive to frequency between $0.01 \text{ Hz} \leq \omega \leq 50$ Hz at $T =$ 25 and 55 °C (Fig. S6). We note that the elastic moduli $G'(\omega)$ for the H_I^{193} and G_I phases differ by one order of magnitude, and that there are significant differences in the frequency-dependent viscous modulus $G''(\omega)$ for these phases. We speculate that these differences arise from differences in water contents of these LLC phases and the preferred deformation axes within these Maxwellian solids; however, the shear rheology of LLCs is quite poorly understood. While this analysis is not necessarily definitive, the frequency-independent nature of $G'(\omega)$ strongly suggests that the H_I^{193} phase is triply periodic.

Since the nanoscale feature sizes and non–covalent, water–laden nature of the new H_I^{193} LLC phase prohibited its direct, real–space imaging by transmission electron microscopy (TEM), we used the high–resolution SAXS pattern in Fig. 4 to reconstruct an electron density map of this phase. Rietveld refinement of this SAXS pattern using the $P6_3/mcm$ space group symmetry in the *JANA2006*[18] software package enabled extraction of the observed structure factor intensities (Fig. S7 and Table S2). Using these data as inputs for the charge–flipping algorithm *SUPERFLIP*,[19, 26] we obtained an excellent fit of the experimental diffraction pattern from which we reconstructed the electron density contrast map shown in Fig. 5a (for details see Supporting Information Fig. S10). This map illustrates the labyrinthine nature of the H_I^{193} phase, which confirms its triply periodic network morphology. An idealized wireframe drawing of the tetracontinuous H_I^{193} structure in Fig. 5b depicts the three identical, non–intersecting and interpenetrating lipid networks within a matrix of water as the fourth network. Each of the three lipid networks in the H_I^{193} phase is an [8,3]–net with $P6_3/mmc$ symmetry (space group #194), fashioned from three–fold connectors with either 0° or 90° dihedral angles between them (Fig. 5c). The [8,3]–net designation in Wells' notation in refers to the fact that each symmetric network is comprised of 8–membered rings of three–fold connectors. This unusual structure is also referred to as the ***3–etc*** net.[14] Note that the G_I–phase formed upon heating the H_I^{193} network above 80 °C comprises two interpenetrating lipid networks in a matrix of water, wherein each network is a [10,3]–net comprised of three–fold connectors with a 70.5° dihedral angle between them.[27] The formation of three–fold connectors in these network LLCs is consistent with their lower degrees of packing frustration and smaller deviations from constant mean interfacial curvature, as compared to higher valency four– and six–fold connectors.[28]

While true epitaxial relationships between the H_I^{193} phase and the adjacent C_I and G_I phases cannot be rigorously deduced from our SAXS data, the H_I^{193} model suggests some structural features that correlate with quantitative crystallographic

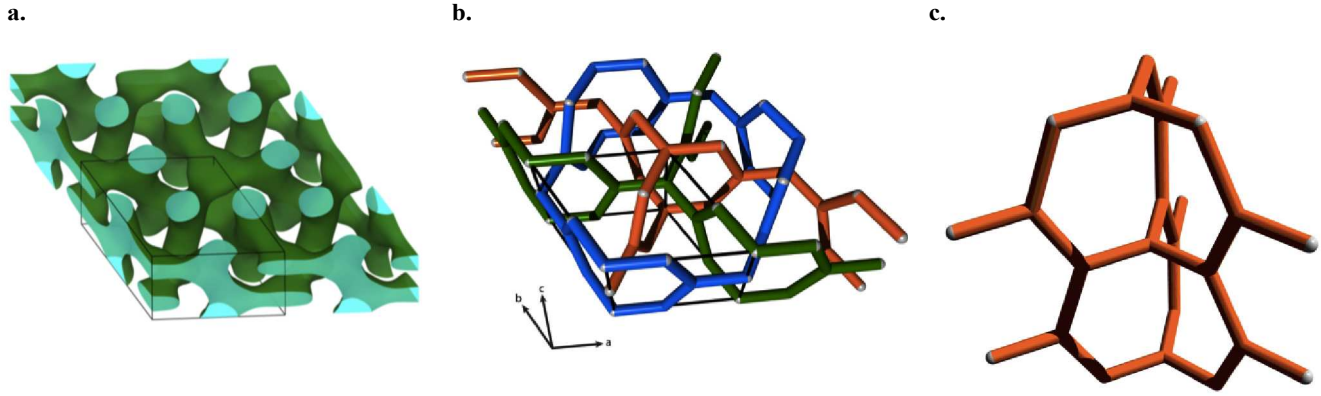

Figure 5. (a) Structural models for the tetracontinuous H_I^{193} phase LLC. (A) Electron density reconstruction derived from the SAXS pattern in Fig. 2B, derived from Rietveld refinement of the data and subsequent use of the charge flipping algorithm *SUPERFLIP*. (b) An idealized wire-frame model of the three interpenetrating and non-intersecting lipidic [8,3]-nets (***3-etc***) with overall $P6_3/mcm$ symmetry, in which each network is colored for visual clarity. (c) A wire-

frame model of a single [8,3]-net, which exhibits $P6_3/mmc$ symmetry (see text for details).

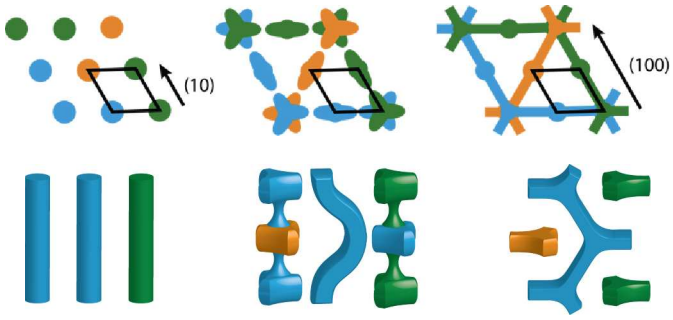

Fig. 6. Schematic depiction of the structural relationships between the C_I and H_I^{193} phases. (*Top*) A unit cell projection along the C_I phase *c*-axis, with an embedded black rhombus that outlines the unit cell, shows that the intercylinder distance is half of the unit cell dimension *a* for the tetracontinuous H_I^{193} network phase. Arrows indicate (10) and (100) lattice vectors of the C_I and H_{I193} phases respectively. (*Bottom*) In a unit cell projection along the *a*-axis of the C_I-phase, dehydration of the results in the regular buckling and pinching off of the cylinders to form the three networks of three-fold connectors in the H_I^{193} phase.

relationships apparent in the SAXS data in Fig. 2. The (100) reflection at q = 0.0908 Å^{-1} of the H_I^{193} network that corresponds to the unit cell *a* parameter occurs at nearly one half of the value of the (10) reflection of the coexisting C_I phase (q = 0.186 Å^{-1}) in the LLC composed of 55.0 wt% **Na–94** (Fig. 2b). Thus, the *a*–axis dimension of the H_I^{193} phase is nearly double that of the intercylinder distance in the C_I–phase. This relationship suggests that removing water from the C_I–phase results in: (1) regular buckling of every other lipid cylinder to form the zig–zag pattern of connectors running parallel to the *c*–axis (0° dihedral angle between connectors), while (2) the remaining lipid cylinders pinch off to form the stacks of staggered, three–fold connectors that connect the buckled cylinders (Fig. 6). This morphological relationship only holds if the H_I^{193} phase is comprised of three interpenetrating lipid networks. The staggered stacking of three–fold connectors along the *c*–axis of the H_I^{193} LLC is also reminiscent of the stacking of staggered connectors along the (111) axis of the G_I–phase. The distance between these stacks in the H_I^{193} phase is *a* = 7.34 nm, which is similar to the unit cell parameter *a* = 7.60 nm for the coexisting G_I–phase at 60.0 wt% **Na–94** (Fig. 2c). The difference in these values probably arises from the substantial differences in network connectivity and symmetry between these two phases. Efforts to prepare highly–oriented pseudo–"single crystal" samples of the H_I^{193} phase for careful studies of these proposed morphological relationships have been thus far unsuccessful.

Aside from the ubiquity of C-phase LLCs with 2D–hexagonal *P6/mm* symmetry (space group #183), LLCs with 3D-hexagonal symmetries are quite rare. Impéror-Clerc and co-workers previously reported the observation of a discontinuous micellar Type I LLC phase with $P6_3/mmc$ symmetry (space group #194), comprising hexagonally-closest packed spherical micelles derived from a non-ionic surfactant.[29, 30] In a related report, Seddon and co-workers more recently described the discovery the corresponding Type II LLC in which reverse spherical micelles form a hexagonally-closest packed lattice.[31] Thus, our observation of the H_I^{193} LLC constitutes only the third report of an LLC with 3D-hexagonal symmetry and the first hexagonal network phase.

Schröder–Turk and Hyde posited the existence of a variety of triply periodic multiply continuous network LLCs with mean interfacial curvatures in between those of the L_α and the C–phases.[16] However, non–cubic, network phases in self–assembling soft materials are exceedingly rare, having been only recently observed in block copolymers.[32-34] Only the cubic G, D, and P network phase LLCs have been previously observed in simple lipid/water mixtures, leading to speculations that the ubiquity of cubic LLCs stems from their intrinsically low degrees of packing frustration.[3] Schröder–Turk combined geometric packing arguments with calculations of the bending rigidity and stretching frustrations associated with lipids packed on the Schwarz H minimal surface to predict the stability of an inverse (Type II) network LLC with $P6_3/mmc$ symmetry.[35] More sophisticated calculations later revealed that the inverse $P6_3/mcm$ structure with mean interfacial curvature between that of the G_{II} and H_{II} phases is a more likely LLC candidate in H_2O.[14] However, these analyses are only indirectly relevant to the normal H_I^{193} phase reported here.

In 2009, Ying and co–workers used electron diffraction TEM studies of a few well–ordered particles of their newly synthesized mesoporous silicate IBN–9 to identify its underlying $P6_3/mcm$ symmetry.[9] Formed from a complex mixture of a silicate precursor, NH_4OH, H_2O, and a 4° ammonium surfactant likely under non–equilibrium conditions, IBN–9 consists of a single silicate sheet that partitions space into three equivalent [8,3]–networks. Thus, IBN–9 is structurally analogous to the aqueous matrix of our H_I^{193} LLC phase. While the formation of the IBN–9 structure indirectly suggests the formation of the normal H_I^{193}, our data constitutes the first direct observation of the H_I^{193} phase as an equilibrium structure in simple lipid/water mixtures.

Conclusions

The discovery of the tetracontinuous H_I^{193} network phase in gemini dicarboxylate surfactant LLCs establishes that the gemini architecture is a powerful molecular design motif for stabilizing both known and new triply periodic multiply continuous morphologies in self–assembled soft materials. Careful comparison of the previously reported **Na–74** and **Na–76** LLC phase diagrams[17] with that of **Na–94** strongly suggests that: (1) longer aliphatic linkers between the surfactant tails destabilize constant mean interfacial curvature phases such as L_α and H_I, and (2) longer aliphatic surfactant tails drive formation of constant mean curvature phases. Therefore, tuning the molecular aspect ratio of a gemini amphiphile specified by

the relative lengths of the surfactant linker and tails provides enticing opportunities for subtly adjusting LLC interfacial curvature to discover new, triply periodic multiply continuous LLC morphologies with percolating and chemically well-defined nanopores. Initial atomistic molecular dynamics simulations of gemini surfactant self-assembly have revealed the complex interplay of intramolecular headgroup repulsions in defining preferred, anisotropic surfactant conformations that undergo supramolecular packing into non-constant curvature LLCs as specified by the extent of counterion-headgroup association.[23] We anticipate that the "gemini" molecular design principle may extend to the formation of new technologically useful triply periodic network phases in other classes of self–assembling soft materials, including oligomeric and polymeric surfactants as well as block copolymers.

Acknowledgments

We gratefully acknowledge financial support from the National Science Foundation (CHE–1152347), the University of Wisconsin–Madison, and a 3M Corporation Graduate Fellowship to G.P.S. This work also made use of critical core facilities funded in part by NSF grants (CHE–9974839), and the the University of Wisconsin NSEC (DMR–0425880 and DMR–0832760) and CEMRI (DMR–0520527 and DMR–1121288), which are part of the NSF–funded Materials Research Facilities Network. Synchrotron SAXS studies were conducted at Sector 12 of the Advanced Photon Source at Argonne National Laboratory, which is supported by the U.S. DOE (Contract #DE–AC02–06CH11357).

Notes and References

Department of Chemistry, University of Wisconsin–Madison, 1101 University Ave., Madison, WI 53706. Email: mahesh@chem.wisc.edu

† Electronic Supplementary Information (ESI) available: SAXS data and associated tables, rheological measurements and details of electron density reconstruction method. See DOI: 10.1039/b000000x/

1. T. Kato, N. Mizoshita and K. Kishimoto, *Angew. Chem., Int. Ed.*, 2006, **45**, 38-68.
2. V. Luzzati and P. A. Spegt, *Nature*, 1967, **215**, 701-704.
3. D. M. Anderson, S. M. Gruner and S. Leibler, *Proc. Natl. Acad. Sci. U. S. A.*, 1988, **85**, 5364-5368.
4. S. T. Hyde, in *Handbook of Applied Surface and Colloid Chemistry*, ed. K. Holmberg, John Wiley & Sons, Inc., New York, 2001, vol. 1, pp. 299-332.
5. C. V. Kulkarni, T.-Y. Tang, A. M. Seddon, J. M. Seddon, O. Ces and R. H. Templer, *Soft Matter*, 2010, **6**, 3191-3194.
6. D. L. Gin, C. S. Pecinovsky, J. E. Bara and R. L. Kerr, *Struct Bond*, 2008, **128**, 181-222.
7. D. L. Gin, J. E. Bara, R. D. Noble and B. J. Elliott, *Macromol. Rapid Commun.*, 2008, **29**, 367-389.
8. Q. Huo, D. I. Margolese, U. Ciesla, P. Feng, T. E. Gier, P. Sieger, R. Leon, P. M. Petroff, F. Schuth and G. D. Stucky, *Nature*, 1994, **368**, 317-321.
9. Y. Han, D. Zhang, L. L. Chng, J. Sun, L. Zhao, X. Zou and J. Y. Ying, *Nat Chem*, 2009, **1**, 123-127.
10. V. Cherezov, *Curr. Opin. Struct. Biol.*, 2011, **21**, 559-566.
11. V. Cherezov, D. M. Rosenbaum, M. A. Hanson, S. G. F. Rasmussen, F. S. Thian, T. S. Kobilka, H.-J. Choi, P. Kuhn, W. I. Weis, B. K. Kobilka and R. C. Stevens, *Science*, 2007, **318**, 1258-1265.
12. C. Leal, N. F. Bouxsein, K. K. Ewert and C. R. Safinya, *J. Amer. Chem. Soc.*, 2010, **132**, 16841-16847.
13. P. T. Spicer, *Curr. Opin. Colloid. Interface Sci.*, 2005, **10**, 274-279.
14. G. E. Schroder-Turk, L. de Campo, M. E. Evans, M. Saba, S. C. Kapfer, T. Varslot, K. Grosse-Brauckmann, S. Ramsden and S. T. Hyde, *Faraday Discuss.*, 2013, **161**, 215-247.
15. S. Andersson, S. T. Hyde, K. Larsson and S. Lidin, *Chemical Reviews*, 1988, **88**, 221-242.
16. S. T. Hyde and G. E. Schröder, *Curr. Opin. Colloid. Interface Sci.*, 2003, **8**, 5-14.
17. G. P. Sorenson, K. L. Coppage and M. K. Mahanthappa, *J. Am. Chem. Soc.*, 2011, **133**, 14928-14931.
18. *Jana2006*–The Crystallographic Computing System, 2006, http://jana.fzu.cz
19. L. Palatinus and G. Chapuis, *J. Appl. Crystallogr.*, 2007, **40**, 786-790.
20. B. A. Pindzola, J. Jin and D. L. Gin, *J. Am. Chem. Soc.*, 2003, **125**, 2940-2949.
21. M. In and R. Zana, *J. Disper. Sci. Technol.*, 2007, **28**, 143-154.
22. E. S. Hatakeyama, B. R. Wiesenauer, C. J. Gabriel, R. D. Noble and D. L. Gin, *Chem. Mater.*, 2010, **22**, 4525-4527.
23. J. Mondal, M. Mahanthappa and A. Yethiraj, *J. Phys. Chem. B*, 2013, **117**, 4254-4262.
24. T. Hahn, U. Shmueli, A. J. C. Wilson and International Union of Crystallography., *International Tables for Crystallography*, John Wiley & Sons, Ltd., Chichester, U. K., 2011.
25. R. Mezzenga, C. Meyer, C. Servais, A. I. Romoscanu, L. Sagalowicz and R. C. Hayward, *Langmuir*, 2005, **21**, 3322-3333.
26. J. Wu, K. Leinenweber, J. C. H. Spence and M. O'Keeffe, *Nature Mater.*, 2006, **5**, 647-652.
27. S. Foerster, A. K. Khandpur, J. Zhao, F. S. Bates, I. W. Hamley, A. J. Ryan and W. Bras, *Macromolecules*, 1994, **27**, 6922-6935.
28. M. W. Matsen and F. S. Bates, *Macromolecules*, 1996, **29**, 7641-7644.
29. M. Clerc, *J. Phys. II France*, 1996, **6**, 961-968.
30. X. Zeng, Y. Liu and M. Impéror-Clerc, *The Journal of Physical Chemistry B*, 2007, **111**, 5174-5179.
31. G. C. Shearman, A. I. I. Tyler, N. J. Brooks, R. H. Templer, O. Ces, R. V. Law and J. M. Seddon, *J. Am. Chem. Soc.*, 2009, **131**, 1678-1679.
32. T. H. Epps, E. W. Cochran, T. S. Bailey, R. S. Waletzko, C. M. Hardy and F. S. Bates, *Macromolecules*, 2004, **37**, 8325-8341.
33. E. W. Cochran and F. S. Bates, *Phys. Rev. Lett.*, 2004, **93**, 087802.
34. A. J. Meuler, M. A. Hillmyer and F. S. Bates, *Macromolecules*, 2009, **42**, 7221-7250.
35. G. E. Schroder-Turk, T. Varslot, L. de Campo, S. C. Kapfer and W. Mickel, *Langmuir*, 2011, **27**, 10475-10483.

TOC GRAPHIC–FOR TABLE OF CONTENTS USE ONLY

An aliphatic gemini dicarboxylate surfactant is shown to form a new 3D-hexagonal lyotropic liquid crystalline phase with *P6₃/mcm* symmetry.

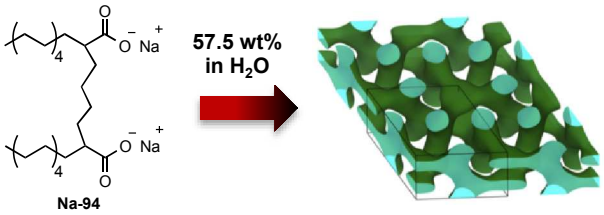

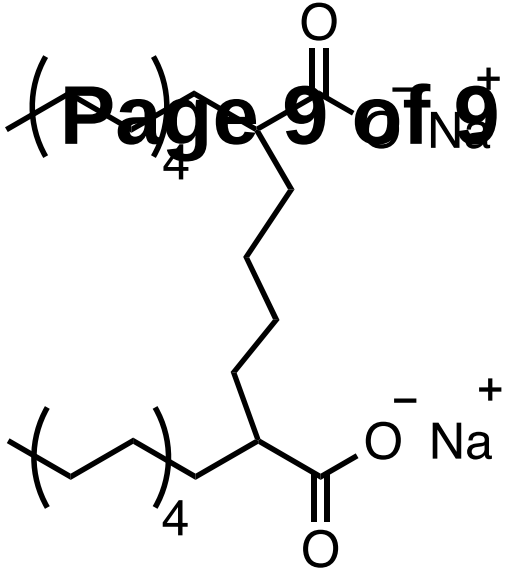

Na-94

57.5 wt%
in H_2O